Article

Conductive Nanosheets Fabricated from Au Nanoparticles on Aqueous Metal Solutions under UV Irradiation

Maho Tagawa , Hiroto Kaneki , Takeshi Kawai *

Posted Date: 27 December 2023

doi: 10.20944/preprints202312.2090.v1

Keywords: Au nanoparticles; UV irradiation; conductive nanosheets; air-water interface

Article

Conductive Nanosheets Fabricated from Au Nanoparticles on Aqueous Metal Solutions under UV Irradiation

Maho Tagawa [1], Hiroto Kaneki [1] and Takeshi Kawai [1,*]

Department of Industrial Chemistry, Tokyo University of Science, 6-3-1 Niijuku, Katsushika-ku, Tokyo 125-8585, Japan; kawai@ci.tus.ac.jp (T.K.)

* Correspondence: kawai@ci.tus.ac.jp; Tel.: +81-358761654

Abstract: Highly transparent, conductive nanosheets are extremely attractive for advanced optoelectronic applications. Previously, we have demonstrated that transparent, conductive Au nanosheets can be prepared by UV irradiation of Au nanoparticle (AuNP) monolayers spread on water, which serves as the subphase. In this study, we show that this UV irradiation technique can easily be extended as a nanosheet modification method by using subphases containing metal ions. That is, aqueous solutions containing Au and Ag ions are effective in modifying Au nanosheets. $HAuCl_4$ solutions increased Au nanosheet thickness, which improved conductivity, but reduced transparency. On the other hand, use of aqueous $AgNO_3$ and CH_3COOAg solutions yielded Au-Ag hybrid nanosheets; however, their morphologies depended on the electrolytes used. Homogeneous Au-Ag nanosheets from $AgNO_3$ and AuNPs covered with an Ag nanosheet from CH_3COOAg were also produced. Further, these Au-Ag hybrid nanosheets had high conductivity without reduced transparency. Therefore, this UV irradiation method, modified by adding metal ions is quite effective at improving and diversifying properties of Au nanosheets.

Keywords: Au nanoparticles; UV irradiation; conductive nanosheets; air-water interface

1. Introduction

Transparent conductive materials are essential components of advanced optical and electronic devices [1–10]. Fluorine- or indium-doped tin oxide films are the most commonly used transparent conducting materials, but they have low flexibility and are brittle [11–14]. Noble metal nanoparticles (NPs) have attracted attention as alternative materials. For example, flexible transparent conductive films have been fabricated by arranging NPs in grid-like patterns on appropriate substrates [3,4,15–18]. However, post-processing surfaces of NPs is essential to removing insulating organic compounds to make the grids conductive [4,17–20]. Despite the requirement for post-processing, this method remains appealing for fabricating transparent conductive films due to the availability of various synthesis protocols for desired sizes of metal NPs.

In previous papers, we have demonstrated that UV irradiation of non-conductive AuNP monolayers at the air-water interface can be converted into flexible, transparent, conductive Au nanosheets [21,22]. In this process, the key to conversion by UV irradiation is photodecomposition of capping molecules covering AuNPs to form an unstable, bare Au surface, and aggregation and fusion phenomena at those surfaces. Here, fusion of AuNPs depends on their size. Small particles fuse easily, but the fusion process is less likely to proceed with larger particles. Actually, in a previous study we demonstrated that UV irradiation of monolayers of AuNPs with 30 nm in diameter created connections among them, but they did not fuse sufficiently, resulting in nanosheets that retain the shapes of the particles [22]. On the other hand, AuNPs with diameters 15 nm or less gave rise to flat nanosheets of uniform thickness, indicating that fusion between AuNPs was sufficient. Accordingly, this UV irradiation technique appears to be inapplicable for larger AuNPs. Nanosheets made from these larger particles exhibit high mechanical strength and conductivity, although their conductivity and mechanical strength is inversely related to their transparency.

 doi:10.20944/preprints202312.2090.v1

To further develop this UV irradiation technique, a strategy is needed to produce nanosheets with various thicknesses and compositions from a single type of metal nanoparticle monolayer. In this study, we propose a UV irradiation technique for preparing thick Au nanosheets from a single type of AuNP by replacing the water subphase with aqueous solutions of $HAuCl_4$. Furthermore, we demonstrate that using $AgNO_3$ and CH_3COOAg gives rise to Au-Ag nanosheets with high conductivity and transparency and we show that their morphologies depend on the electrolytes chosen. Au-Ag nanosheets prepared from $AgNO_3$ have homogeneous flat structures, while those from CH_3COOAg have the structure of AuNPs embedded in an Ag thin film.

2. Materials and Methods

2.1. Materials

Silver acetate (CH_3COOAg), silver nitrate ($AgNO_3$), sodium borohydride ($NaBH_4$), and chloroform were obtained from Kanto Chemical Co., Inc. Gold (III) chloride trihydrate ($HAuCl_4 \cdot 3H_2O$), tetraoctylammonium bromide (TOAB), and dodecanethiol (DDT) were purchased from Nacalai Tesque Inc., Tokyo Chemical Industry Co., Ltd. and Sigma-Aldrich, respectively. All chemicals were used as received, without further purification.

2.2. Preparation of Au nanoparticles (AuNPs)

AuNPs capped with DDT were prepared using a modified Brust-Schiffrin method [23]. A 0.384 mmol $HAuCl_4$ aqueous solution (7.91 mL) was added to a 0.362 mmol phase-transfer reagent, TOAB, dissolved in toluene (7.91 mL), and the mixture was stirred for 15 min or until the aqueous phase was clear. The toluene phase, containing phase-transferred gold, was subsequently collected and a 0.066 mmol DDT solution in toluene (1.51 mL) was added. After the solution was stirred for 1 h, a freshly prepared 4.22 mM solution of $NaBH_4$ in water (2 mL) was quickly added with high stirring to reduce the Au ions. The reaction mixture was vigorously stirred for 12 h to allow formation of AuNPs and the organic phase was isolated. As-prepared AuNPs were then dispersed in DDT (2.54 mL), and the dispersion was refluxed at 80 °C for 22 h. In order to remove excess DDT, AuNPs in DDT were washed thoroughly several times with acetone through centrifugal separation. Purified AuNPs were dispersed in chloroform. AuNPs had a spherical shape and an average diameter of 4.7 ± 0.5 nm.

2.3. Preparation of Au and Au-Ag nanosheets

A suspension of purified AuNPs in chloroform was spread on water and compressed using a Teflon barrier until AuNPs were organized into a close-packed structure. The AuNP monolayer was moved onto an aqueous solution of $HAuCl_4$, $AgNO_3$ or CH_3COOAg, and the AuNP monolayer was irradiated with UV light through an optical fiber (Figure 1). Au nanosheets were prepared by UV irradiation of a close-packed AuNP monolayer prepared on water without transferring it to another aqueous solution. UV light from a 250 W mercury lamp (REX-250, Asahi Spectra Co., Ltd.) was passed through a narrow band optical filter to obtain 248-nm UV light. Samples were irradiated with 248-nm UV light at an intensity of ≈60 mW cm^{-2}.

2.4. Characterization

To characterize Au nanosheets, as-prepared Au or Au-Ag nanosheets on aqueous solutions were transferred from the water surface to various solid substrates using the surface lowering method: (i) copper grids coated with an elastic carbon film for transmission electron microscopy (TEM), (ii) glass slides for scanning electron microscopy (SEM), X-ray diffraction measurements (XRD) and electrical resistivity measurements, (iii) quartz plates for UV-vis analysis, and (iv) quartz crystal chips for quartz crystal microbalance (QCM) measurements.

TEM images were taken using a JEOL JEM-1101 microscope operated at 100 kV. Energy dispersive x-ray spectroscopy (EDS) mapping images and scanning TEM images were captured using a JEOL JEM-2100 microscope operated at 200 kV. SEM images were obtained on a Carl Zeiss JEM-

Preprints (www.preprints.org) | NOT PEER-REVIEWED | Posted: 27 December 2023 doi:10.20944/preprints202312.2090.v1

2100 microscope operating at 8 kV. UV-visible spectra were acquired on a JASCO V-780 UV-vis spectrophotometer. X-ray diffraction (XRD) measurements were performed using a diffractometer (Rigaku, Ultima IV). Electrical resistivity of nanosheets deposited on the glass substrates was measured using a four-probe method with a digital multimeter (NF Corporation, DM2561A) and four-point probe (Astellatech, Inc.), where the spacing between adjacent probes was 1 mm.

Masses of Au and Au-Ag nanosheets transferred onto 9 MHz AT-cut chips (SEIKO EG&G, QA-A9M-AU) were monitored using the QCM SYSTEM (SEIKO EG&G, QCM922). Masses of nanosheets were evaluated using the following Sauerbrey equation [24,25]:

$$\Delta F = -\frac{2\Delta m f_0^2}{A\sqrt{\mu_q \rho_q}}$$

where ΔF is the measured frequency change (Hz), f_0 is the fundamental frequency, Δm is the mass change (g), A is the electrode area (cm^2), ρ_q is the density of quartz (2.65 g cm^{-3}), and μ_q is the shear modulus of quartz (2.95×10^{11} g cm^{-1} s^{-2}).

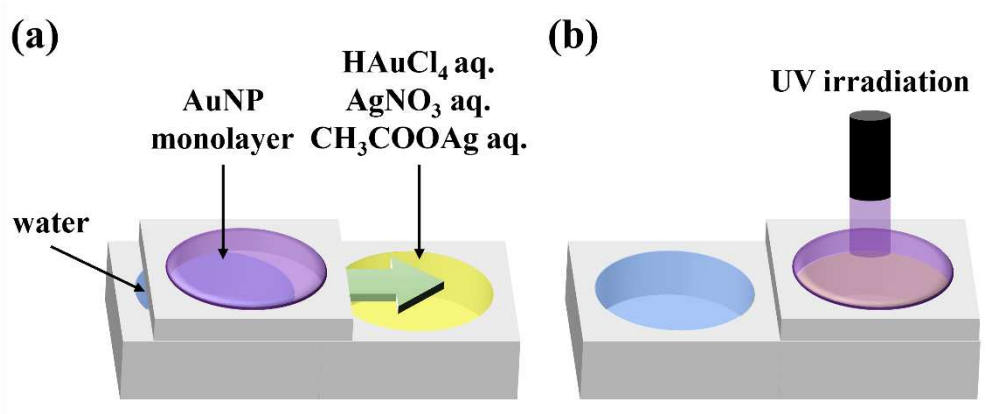

Figure 1. Schematic illustration of the experimental procedure. (a) AuNP monolayers are prepared by spreading a chloroform dispersion of AuNPs on water. The AuNP monolayer is then transferred onto an aqueous solution of $HAuCl_4$, $AgNO_3$ or CH_3COOAg, and (b) irradiated with UV light.

3. Results

3.1. Preparation of thick Au nanosheets

AuNP monolayers were prepared by spreading a chloroform dispersion of DDT-capped AuNPs (4.7 ± 0.5 nm) on water, and the monolayer was irradiated with UV light for 60 min. AuNPs in the monolayer were transformed into a mesh-like Au nanosheet (Figure 2a), as reported previously [21]. To investigate effects of metal species in water on formation of Au nanosheets, after preparing an AuNP monolayer on water, the monolayer was moved onto an aqueous $HAuCl_4$ solution and then the monolayer was irradiated with UV light. Figures 2b-d show TEM images of resultant Au nanosheets prepared on 4.8, 48 and 480 μM aqueous $HAuCl_4$ solutions. All AuNP monolayers were transformed into mesh-like Au nanosheets upon UV irradiation. However, the mesh size varied significantly with the concentration of $HAuCl_4$. The width of the mesh prepared on water was 9.5 ± 2.8 nm, whereas those on 48 and 480 μM $HAuCl_4$ solutions were 25.8 ± 7.8 and 81.9 ± 29.5 nm, respectively. This increase in mesh size was also apparent in SEM images (Figure 3).

Preprints (www.preprints.org) | NOT PEER-REVIEWED | Posted: 27 December 2023 doi:10.20944/preprints202312.2090.v1

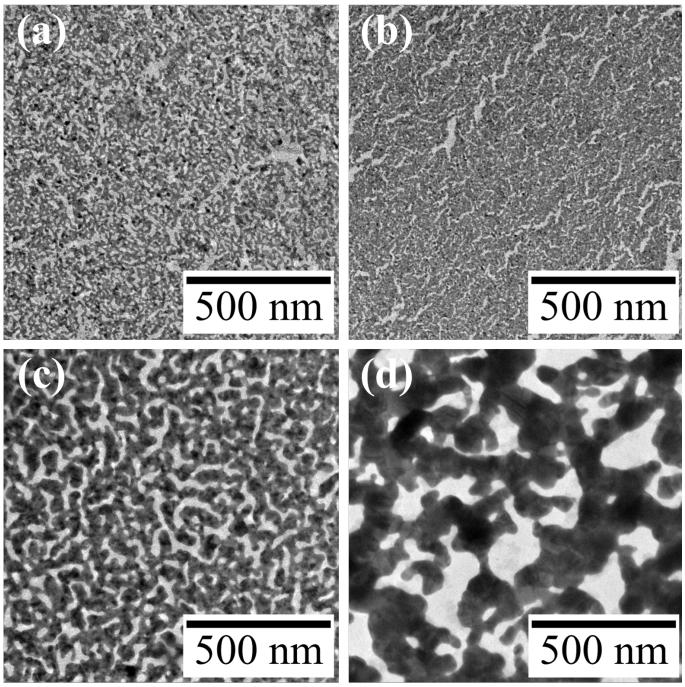

Figure 2. TEM images of Au nanosheets prepared on (a) water, (b) 4.8-, (c) 48- and (d) 480-μM $HAuCl_4$ aqueous solutions.

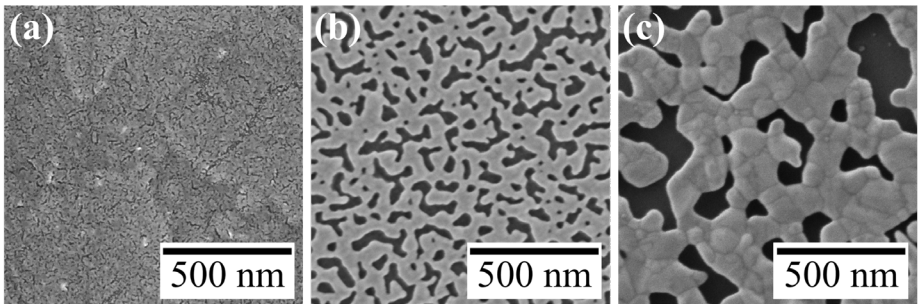

Figure 3. SEM images of Au nanosheets prepared on (a) 4.8-, (b) 48- and (c) 480-μM $HAuCl_4$ aqueous solutions.

Figure 4 shows TEM images of UV irradiated AuNP monolayers on water and aqueous $HAuCl_4$ solutions as a function of time. After 15 min of UV irradiation, AuNPs on water remained almost unchanged, but those on $HAuCl_4$ solutions transformed completely into larger aggregates. In particular, on 480-μM $HAuCl_4$ solution, the morphological change of AuNPs was remarkable. Hence, $HAuCl_4$ promotes morphological transformation of AuNPs to nanosheets.

To characterize Au nanosheets, XRD, electrical resistance and transmittance in the visible region were measured. Figure 5 shows the XRD pattern of a nanosheet prepared on a 480-μM $HAuCl_4$ solution. The nanosheet was confirmed as crystalline gold, based on reflection peaks at 38.2°, 44.3°, 64.5°, 77.5° and 81.7°, which were assigned to the (111), (200), (220), (311) and (222) crystal facets of Au, respectively, with a face-centered cubic structure [26,27]. Electrical resistances of Au nanosheets prepared on water, 48 μM and 480 μM $HAuCl_4$ solutions were 2600 Ω/sq, 6.5 Ω/sq and 4.1 Ω/sq, respectively. Electrical resistances of Au nanosheets prepared on $HAuCl_4$ solutions were considerably smaller, which can be explained by the increase in film thickness, as evaluated by QCM measurements. Hence, we demonstrated that Au nanosheets with high electrical conductivity can be prepared using a single type of AuNP, avoiding the necessity of synthesizing new AuNPs with different diameters.

Preprints (www.preprints.org) | NOT PEER-REVIEWED | Posted: 27 December 2023 doi:10.20944/preprints202312.2090.v1

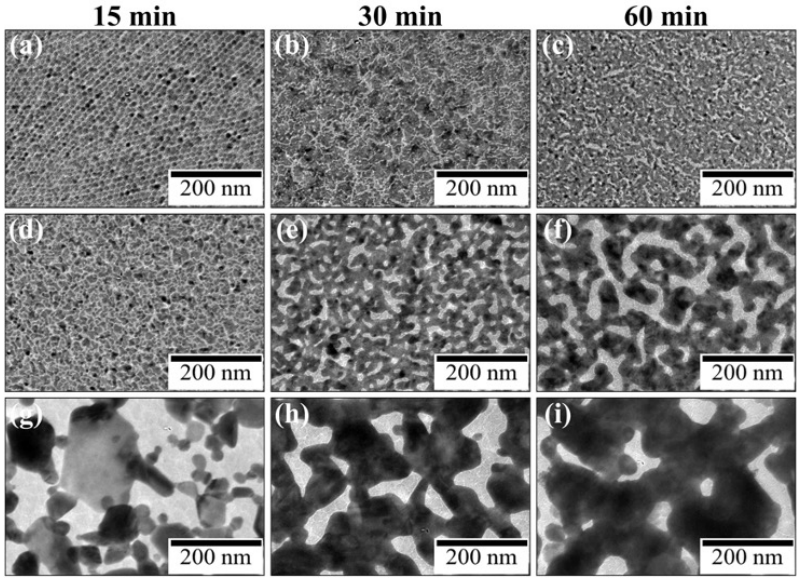

Figure 4. TEM images of Au nanosheets prepared on (a-c) water, (d-f) 48- and (g-i) 480-μM $HAuCl_4$ aqueous solutions at irradiation times of (a,d,g) 15, (b,e,h) 30, and (c,f,i) 60 min.

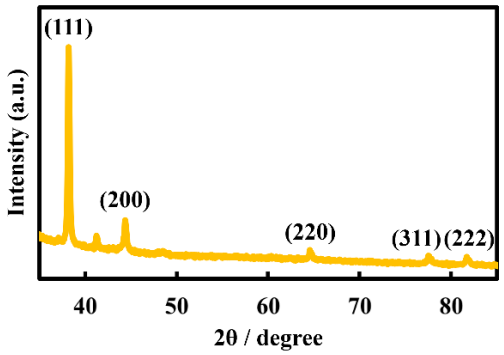

Figure 5. XRD pattern of Au nanosheets prepared on a 480-μM $HAuCl_4$ aqueous solution.

Electrical resistance and transparency are inversely related, and both properties depend strongly on the thickness of Au nanosheets. Thick Au nanosheets possess high electrical conductivity, but low transparency, and vice versa [28,29]. Thus, as a natural consequence, Au nanosheets prepared on $HAuCl_4$ solutions are likely to have low transparency in the visible and UV region. Actually, Au nanosheets prepared on 48-μM and 480-μM $HAuCl_4$ solutions had optical transparencies of 55% and 8%, respectively (Figure 6), whereas the Au nanosheet prepared on water had a transparency of ~80%.

3.2. Preparation of Au-Ag hybrid nanosheets

3.2.1. Effect of $AgNO_3$ and CH_3COOAg

Employing $HACl_4$ solutions as a subphase was useful to modify Au nanosheets prepared by irradiating AuNP monolayers with UV light. This suggested that other metal ions might also be useful for modifying Au nanosheets. We then attempted to prepare Au-Ag nanosheets by irradiating AuNP monolayers on aqueous $AgNO_3$ and CH_3COOAg solutions, using the same method as described above. Figure 7 shows TEM images of UV-irradiated AuNPs on water, aqueous 500 μM $AgNO_3$ and CH_3COOAg solutions. For water and $AgNO_3$ systems (Figure 7a, b, d, e), UV irradiation resulted in complete fusion of AuNPs, yielding flat nanosheets with gaps in which no metal is present, although the gap size and density of the $AgNO_3$ nanosheet were smaller than those on water.

Preprints (www.preprints.org) | NOT PEER-REVIEWED | Posted: 27 December 2023 doi:10.20944/preprints202312.2090.v1

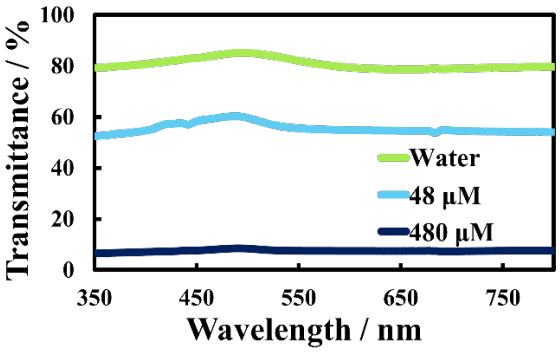

Figure 6. UV-vis spectra of Au nanosheets prepared at various concentrations of $HAuCl_4$ aqueous solution.

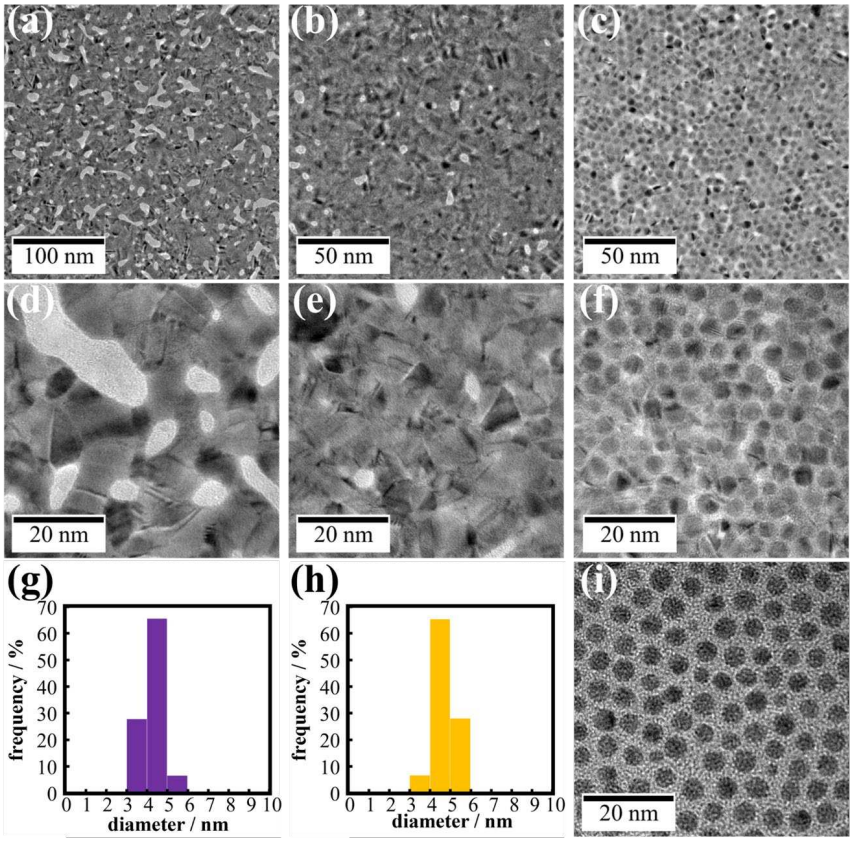

Figure 7. TEM images of Au nanosheets prepared on (a,d) water, (b,e) $AgNO_3$ and (c,f) CH_3COOAg aqueous solutions. Particle size distribution histograms of (g) AuNPs before UV irradiation and (h) AuNPs in a nanosheet prepared on CH_3COOAg aqueous solution. (i) TEM image of AuNPs before UV irradiation.

Reducing the size and density may be attributed to depositing Ag atoms generated by photoredution of Ag^+ ions. Deposition of Ag atoms was confirmed by TEM-EDS (energy dispersive X-ray spectroscopy) mapping. Figure 8a-c show that a nanosheet prepared on aqueous 500 µM $AgNO_3$ is composed of both Ag and Au, and these metals are homogeneously distributed throughout the nanosheet. The molar ratio of Ag to Au in the nanosheet was Ag/Au = 20/80 from TEM-EDS analysis. Further, we measured the XRD pattern of the hybrid nanosheet to determine whether silver is oxidized or whether $AgNO_3$ deposits directly on the nanosheet, although distinguishing between metallic Au and Ag from XRD diffraction is difficult because these metals have nearly identical lattice constants [30]. The XRD pattern in Figure 9a showed reflection peaks at 38.2°, 44.0°, 64.3° and 77.3°, assigned to the (111), (200), (220) and (311) crystal facets of metallic Ag and/or Au, respectively [26,27,31,32]. The absence of silver oxide and $AgNO_3$ peaks suggested that the hybrid nanosheet was

Preprints (www.preprints.org) | NOT PEER-REVIEWED | Posted: 27 December 2023 doi:10.20944/preprints202312.2090.v1

composed of metallic Ag and Au [33,34]. Accordingly, the nanosheet prepared on $AgNO_3$ aqueous solutions is formed by Ag atoms supplied from the aqueous phase, as well as fusion of AuNPs, leading to fewer and smaller gaps.

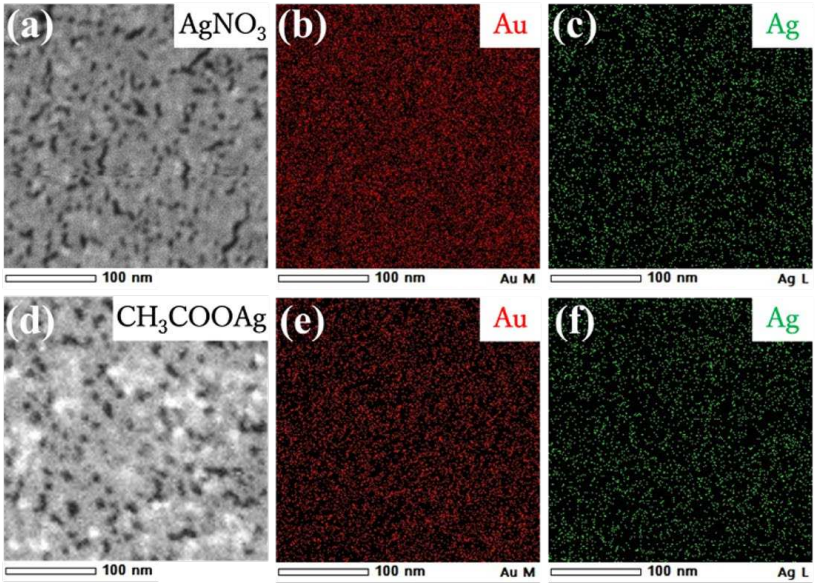

Figure 8. STEM images (a, d) and EDS elemental mapping images (b, c, e, f) of Au-Ag nanosheets prepared on (a-c) $AgNO_3$ and (d-f) CH_3COOAg aqueous solutions.

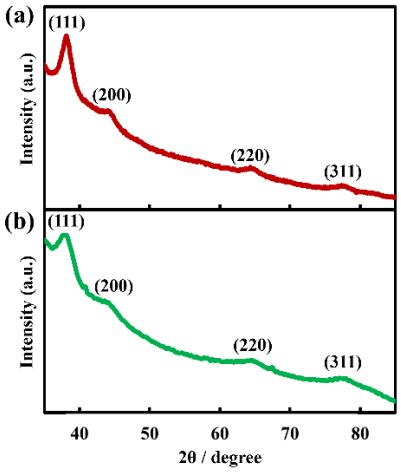

Figure 9. XRD patterns of Au-Ag nanosheets prepared on (a) $AgNO_3$ and (b) CH_3COOAg aqueous solutions.

With regard to the CH_3COOAg system in Figures 7c f, the nanosheet morphology differed significantly from that of the $AgNO_3$ system. Outlines of AuNPs were clearly visible in TEM images of the nanosheet, and AuNPs still remained even after UV irradiation for 60 min. There was no product between AuNPs before UV irradiation (Figure 7i). However, observing TEM images of AuNPs after UV irradiation (Figure 7f), we noticed that AuNPs were connected by a thin film. TEM-EDS mapping (Figure 8b) showed that elemental Ag is present throughout the nanosheet, and TEM-EDS analysis estimated the composition of the hybrid nanosheet as Ag/Au = 40/60. Further, the XRD pattern of the hybrid nanosheets (Figure 9b) showed no peak for silver oxide or CH_3COOAg, and all peaks were assigned to metallic Ag and/or Au. Hence, these TEM-EDS observations and the XRD analysis suggest that metallic silver deposits as a thin film on the entire AuNP monolayer. This assessment is also consistent with the fact that the average diameter of AuNPs remained almost remained unchanged after UV irradiation (Figure 7g, h).

Preprints (www.preprints.org) | NOT PEER-REVIEWED | Posted: 27 December 2023 doi:10.20944/preprints202312.2090.v1

3.2.2. Effect of CH_3COOAg concentration

We demonstrated that UV irradiation of AuNP monolayers on a CH_3COOAg aqueous solution yields a hybrid nanosheet consisting of an AuNP monolayer covered with an Ag thin film, whereas a flat Au nanosheet was obtained on water without CH_3COOAg. Thus, the morphology of these nanosheets is expected to be highly dependent on the CH_3COOAg concentration. The appearance of nanosheets prepared on 5 μM CH_3COOAg was uniform and similar to that prepared on water, (Figure 10a, d). On the other hand, the morphology at 50 μM CH_3COOAg (Figure 10b, e) was not uniform and consisted of two domains. One domain comprised fused AuNPs (red circle in Figure 10e) and the other is AuNPs covered with an Ag thin film (blue circle), similar to that of the 500-μM CH_3COOAg nanosheet (Figure 10c, f). The content of Ag in the hybrid nanosheets was Ag/Au = 19/81 for 5 μM, 35/65 for 50 μM and 40/60 for 500 μM. At low concentrations of CH_3COOAg, formation of uniform nanosheets is probably attributable to preferential fusion between AuNPs, rather than to supplying Ag atoms generated by photoreduction of Ag ions, as shown in Figure 11a. On the contrary, at high concentrations (Figure 10b), since many photoreduced Ag atoms are supplied, prior to fusion of AuNPs, Ag atoms preferentially deposit on AuNPs, which probably inhibits AuNP fusion. Thus, the domain structure at the middle concentration of 50 μM is thought to be driven by competition between Ag deposition on AuNPs and fusion of AuNPs.

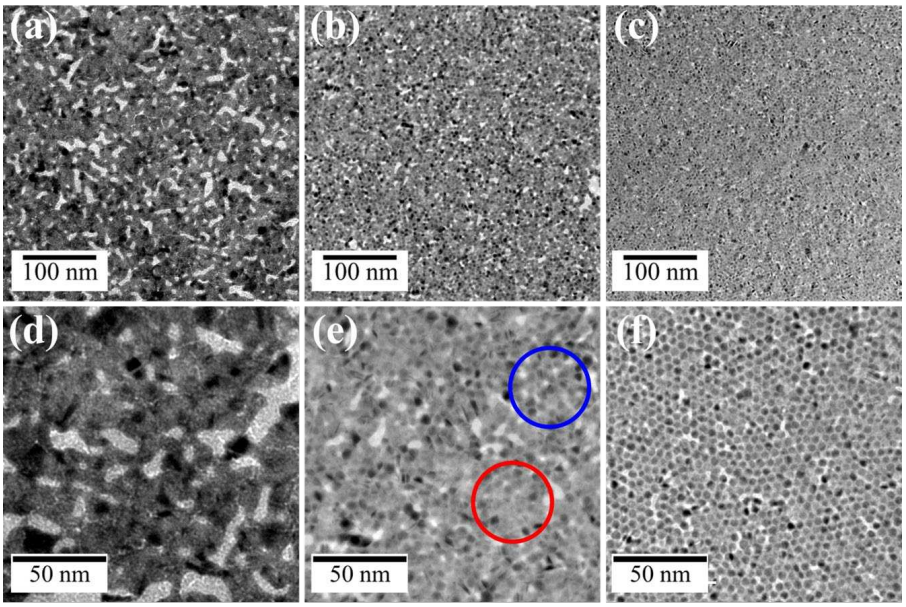

Figure 10. TEM images of Au-Ag nanosheets prepared on (a,d) 5-, (b,e) 50- and (c,f) 500-μM CH_3COOAg aqueous solutions.

We demonstrated that Au-Ag hybrid nanosheets can be prepared on aqueous solutions of $AgNO_3$ and CH_3COOAg, but their morphology differed significantly. As the Ag/Au ratio was 40/60 for the 500-μM CH_3COOAg system and 20/80 for the 500-μM $AgNO_3$ system, this silver content difference probably causes the morphology difference. This is because larger amounts of Ag atoms can cover AuNPs, leading to AuNPs embedded in an Ag film. Why is the supply of Ag atoms in the CH_3COOAg system greater than in the $AgNO_3$ system? According to previous reports [35,36], UV irradiation of aqueous organic molecules, such as alcohols and carboxylic acids, promotes photoreduction of metal ions, because these organic molecules photo-generate radical species that have the potential to reduce metal ions, including Ag. Hence, the larger quantity of reduced Ag in the CH_3COOAg system is because CH_3COO^- ions generate radical species that can reduce Ag ions. Thus, more silver ions are reduced in the CH_3COOAg system than in the $AgNO_3$ system.

Preprints (www.preprints.org) | NOT PEER-REVIEWED | Posted: 27 December 2023 doi:10.20944/preprints202312.2090.v1

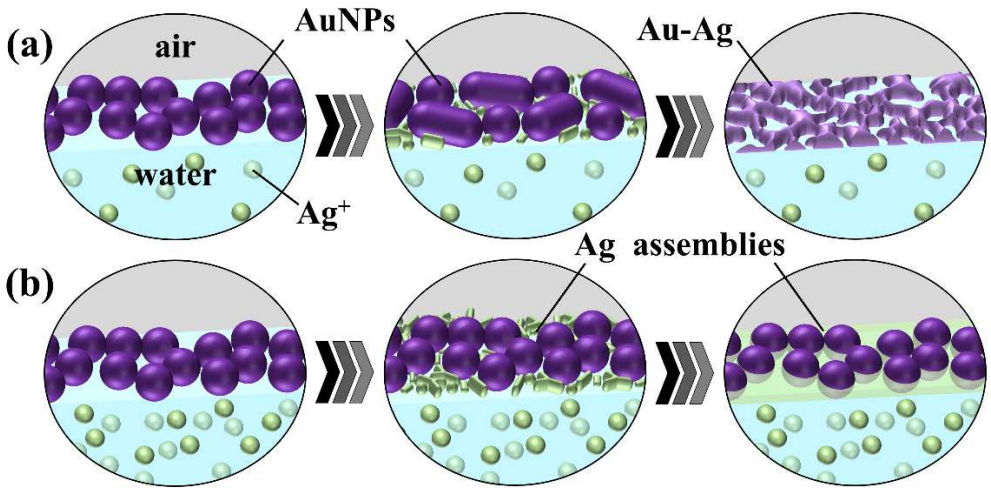

Figure 11. Schematic illustration of proposed growth mechanism of Au-Ag hybrid nanosheets at (a) a low concentration and (b) a high concentration of CH_3COOAg aqueous solutions.

3.3. Conductivity and transparency of Au-Ag hybrid nanosheets

The electrical resistance and optical transmittance of Au-Ag nanosheets were evaluated. Electrical resistances of nanosheets prepared on 500-μM $AgNO_3$ and CH_3COOAg solutions were 1600 Ω/sq and 83 Ω/sq, respectively, smaller than that of the original Au nanosheet (2600 Ω/sq). In particular, the nanosheet prepared on 500-μM CH_3COOAg solution, which has an Ag thin film covering the AuNP monolayer (Figure 7f), had low electrical resistance. On the other hand, transmittances in the UV and visible regions of Au-Ag nanosheets (Figure 12) were almost identical to that of the original Au nanosheet. Hence, covering AuNP monolayers with an Ag thin film improved the conductivity considerably without degrading the transparency. Accordingly, in the process of fabricating transparent conductive films with AuNP monolayers, deposition and coating with silver under UV irradiation proved to be remarkably useful in improving their properties.

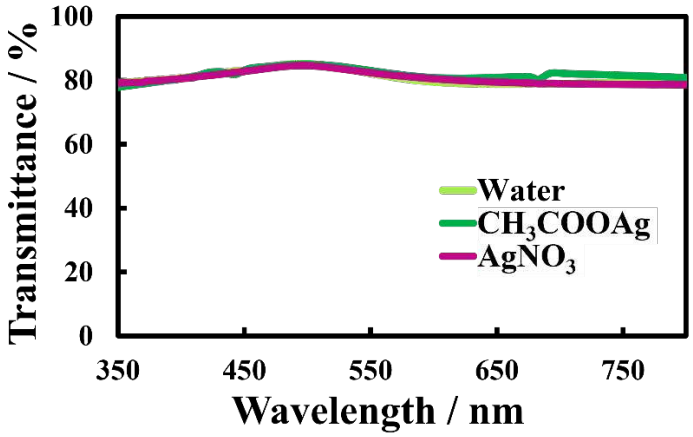

Figure 12. UV-vis spectra of Au-Ag nanosheets prepared on $AgNO_3$ and CH_3COOAg aqueous solutions.

4. Conclusions

We demonstrated that the versatility of a UV irradiation technique for preparing metal nanosheets from metal NP monolayers can be enhanced using subphases containing metal ions. With a single type of AuNP monolayer, using aqueous $HAuCl_4$, $AgNO_3$ and CH_3COOAg solutions as alternative subphases, morphology and composition of Au nanosheets can be changed. Without synthesizing AuNPs of different diameters, one type of AuNP can be used to prepare Au nanosheets with high conductivity, but low transparency using aqueous $HAuCl_4$ solutions. Using aqueous

$AgNO_3$ and CH_3COOAg solutions, Au-Ag nanosheets with high conductivity and transparency can be prepared from the same AuNPs. Further, Au-Ag nanosheets prepared from $AgNO_3$ have a homogeneous flat structure, while those from CH_3COOAg have the structure of AuNPs embedded in an Ag thin film.

Author Contributions: Conceptualization, TK; methodology, MT and HK; investigation, MT, HK and TK; data curation, MT and HK; writing—original draft preparation, MT and TK; writing—review and editing, TK; supervision, TK All authors have read and agreed to the published version of the manuscript.

Funding: This work was supported by JSPS KAKENHI Grant Numbers 19H02538 and 22H01892.

Informed Consent Statement: Not applicable.

Data Availability Statement: Data presented in this study are available on request from the corresponding author, but they are not publicly available because they pertain to an on-going project.

Conflicts of Interest: The authors declare that they have no competing financial interests or personal relationships that could have influenced this work.

References

1. Valasma, R.; Bozo, E.; Pitkänen, O.; Järvinen, T.; Dombovari, A.; Mohl, M.; Lorite, G. S.; Kiss, J.; Konya, Z.; Kordas, K. Grid-Type Transparent Conductive Thin Films of Carbon Nanotubes as Capacitive Touch Sensors. *Nanotechnology* **2020**, *31*, 305303.
2. Nam, V. B.; Shin, J.; Yoon, Y.; Giang, T. T.; Kwon, J.; Suh, Y. D.; Yeo, J.; Hong, S.; Ko, S. H.; Lee, D. Highly Stable Ni-Based Flexible Transparent Conducting Panels Fabricated by Laser Digital Patterning. *Adv. Funct. Mater.* **2019**, *29*, 1806895.
3. Cho, S.; Kang, S.; Pandya, A.; Shanker, R.; Khan, Z.; Lee, Y.; Park, J.; Craig, S. L.; Ko, H. Large-Area Cross-Aligned Silver Nanowire Electrodes for Flexible, Transparent, and Force-Sensitive Mechanochromic Touch Screens. *ACS Nano* **2017**, *11*(4), 4346–4357.
4. Gong, S.; Zhao, Y.; Yap, L. W.; Shi, Q.; Wang, Y.; Bay, J. A. P. B.; Lai, D. T. H.; Uddin, H.; Cheng, W. Fabrication of Highly Transparent and Flexible NanoMesh Electrode via Self-assembly of Ultrathin Gold Nanowires. *Adv. Electron. Mater.* **2016**, *2*(7), 1600121.
5. Lian, L.; Xi, X.; Dong, D.; He, G. Highly conductive silver nanowire transparent electrode by selective welding for organic light emitting diode. *Org. Electron* **2018**, *60*, 9–15.
6. Park, Y.; Bormann, L.; Müller-Meskamp, L.; Vandewal, K.; Leo, K. Efficient Flexible Organic Photovoltaics Using Silver Nanowires and Polymer Based Transparent Electrodes. *Org. Electron* **2016**, *36*, 68–72.
7. Lee, S.; Jang, J.; Park, T.; Park, Y. M.; Park, J. S.; Kim, Y.-K.; Lee, H.-K.; Jeon, E.-C.; Lee, D.-K.; Ahn, B.; Chung, C.-H. Electrodeposited silver nanowire transparent conducting electrodes for thin-film solar cells. *ACS Appl. Mater. Interfaces* **2020**, *12*, 6169–6175.
8. Khaligh, H.H.; Liew, K.; Han, Y.; Abukhdeir, N.M.; Goldthorpe, I.A. Silver nanowire transparent electrodes for liquid crystal-based smart windows. *Sol. Energy Mater. Sol. Cells* **2015**, *132*, 337–341.
9. Wang, B.; Facchetti, A. Mechanically flexible conductors for stretchable and wearable e-skin and e-textile devices. *Adv. Mater.* **2019**, *31*, 1901408.
10. Lee, H.; Hong, S.; Lee, J.; Suh, Y. D.; Kwon, J.; Moon, H.; Kim, H.; Yeo, J.; Ko, S. H. Highly stretchable and transparent supercapacitor by Ag–Au core–shell nanowire network with high electrochemical stability. *ACS Appl. Mater. Interfaces* **2016**, *8* (24), 15449–15458.
11. Kim, C.; Park, J.-W.; Kim, J.; Hong, S.-J.; Lee, M. J. A Highly Efficient Indium Tin Oxide Nanoparticles (ITO-NPs) Transparent Heater Based on Solution-Process Optimized with Oxygen Vacancy Control. *J. Alloys Compd.* **2017**, *726*, 712–719.
12. Kumar, A.; Zhou, C. The Race to Replace Tin-Doped Indium Oxide: Which Material Will Win? *ACS Nano* **2010**, *4*, 11–14.
13. Tran, D.-P.; Lu, H.-I.; Lin, C.-K. Conductive Characteristics of Indium Tin Oxide Thin Film on Polymeric Substrate under Long-Term Static Deformation. *Coatings* **2018**, *8* (6), 212.
14. Chen, Z.; Li, W.; Li, R.; Zhang, Y.; Xu, G.; Cheng, H. Fabrication of Highly Transparent and Conductive Indium–Tin Oxide Thin Films with a High Figure of Merit via Solution Processing. *Langmuir* **2013**, *29* (45), 13836–13842.
15. He, T.; Xie, A.; Reneker, D.H.; Zhu, Y. A Tough and High-Performance Transparent Electrode from a Scalable and Transfer-Free Method. *ACS Nano* **2014**, *8* (5), 4782–4789.
16. Higashitani, K.; Mcnamee, C. E.; Nakayama, M. Formation of Large-Scale Flexible Transparent Conductive Films Using Evaporative Migration Characteristics of Au Nanoparticles. *Langmuir* **2011**, *27* (6), 2080–2083.
17. Kister, T.; Maurer, J. H. M.; González-García, L.; Kraus, T. Ligand-Dependent Nanoparticle Assembly and Its Impact on the Printing of Transparent Electrodes. *ACS Appl. Mater. Interfaces* **2018**, *10* (7), 6079–6083.

18. Maurer, J. H. M.; González-García, L.; Reiser, B.; Kanelidis, I.; Kraus, T. Templated Self-Assembly of Ultrathin Gold Nanowires by Nanoimprinting for Transparent Flexible Electronics. *Nano Lett.* **2016**, *16* (5), 2921–2925.
19. Morag, A.; Philosof-Mazor, L.; Volinsky, R.; Mentovich, E.; Richter, S.; Jelinek, R. Self-Assembled Transparent Conductive Electrodes from Au Nanoparticles in Surfactant Monolayer Templates. *Adv. Mater.* **2011**, *23* (37), 4327–4331.
20. He, Y.; Chen, Y.; Xu, Q.; Xu, J.; Weng, J. Assembly of Ultrathin Gold Nanowires into Honeycomb Macroporous Pattern Films with High Transparency and Conductivity. *ACS Appl. Mater. Interfaces* **2017**, *9* (8), 7826–7833.
21. Nishimura, T.; Ito, N.; Kinoshita, K.; Matsukawa, M.; Imura, Y.; Kawai, T. Fabrication of Flexible and Transparent Conductive Nanosheets by the UV–Irradiation of Gold Nanoparticle Monolayers. *Small* **2020**, *16* (12), 1903365.
22. Matsukawa, M.; Wang, K.-H.; Imura, Y.; Kawai, T. Au Nanoparticle Monolayer Nanosheets as Flexible Transparent Conductive Electrodes. *ACS Appl. Nano Mater.* **2021**, *4* (10), 10845–10851.
23. Brust, M.; Walker, M.; Bethell, D.; Schiffrin, D. J.; Whyman, R. Synthesis of Thiol-Derivatized Gold Nanoparticles in a two-phase Liquid-Liquid system. *Chem. Commun.* **1994**, *7*, 801– 802.
24. Baba, A.; Kaneko, F.; Advincula, R. C. Polyelectrolyte adsorption processes characterized in situ using the quartz crystal microbalance technique: alternate adsorption properties in ultrathin polymer films. *Colloids Surf., A* **2000**, *173*, 39–49.
25. Vogt, B.D.; Lin, E.K.; Wu, W.-I.; White, C.C. Effect of Film Thickness on the Validity of the Sauerbrey Equation for Hydrated Polyelectrolyte Films. *J. Phys. Chem. B* **2004**, *108*, 12685–12690.
26. Imura, Y.; Maniwa, M.; Iida, K.; Saito, H.; Morita-Imura, C.; Kawai, T. Preparing Alumina-Supported Gold Nanowires for Alcohol Oxidation. *ACS Omega* **2021**, *6* (24), 16043–16048.
27. Feng, H.; Yang, Y.; You, Y.; Li, G.; Guo, J.; Yu, T.; Shen, Z.; Wu, T.; Xing, B. Simple and rapid synthesis of ultrathin gold nanowires, their self-assembly and application in surface-enhanced Raman scattering. *Chem. Commun.* **2009**, *15*, 1984–1986.
28. Kwon, J. H.; Jeon, Y.; Choi, K. C. Robust Transparent and Conductive Gas Diffusion Multibarrier Based on Mg- and Al-Doped ZnO as Indium Tin Oxide-Free Electrodes for Organic Electronics. *ACS Appl. Mater. Interfaces* **2018**, *10* (38), 32387–32396.
29. Sun, K.; Li, P.; Xia, Y.; Chang, J.; Ouyang, J. Transparent conductive oxide-free perovskite solar cells with PEDOT:PSS as transparent electrode. *ACS Appl. Mater. Interfaces* **2015**, *7* (28), 15314–15320.
30. Chen, D.; Li, C.; Liu, H.; Ye, F.; Yang, J. Core-shell Au@Pd Nanoparticles with Enhanced Catalytic Activity for Oxygen Reduction Reaction via Core-Shell Au@Ag/Pd Constructions. *Sci. Rep.* **2015**, *5*, 11949.
31. Jiang, H.; Moon, K.-S.; Li, Y.; Wong, C. P. Surface Functionalized Silver Nanoparticles for Ultrahigh Conductive Polymer Composites. *Chem. Mater.* **2006**, *18*, 2969–2973.
32. Kulkarni, A. A.; Bhanage, B. M. Ag@ AgCl nanomaterial synthesis using sugar cane juice and its application in degradation of azo dyes. *ACS Sustainable Chem. Eng.* **2014**, *2*, 1007–1013.
33. Runa, X.; Zhou, S.; Yin, C.; Bai, J.; Zhang, X.; Khan, A.; Xu, A.; Li, X. Insight into the catalytic performance of silver oxides towards peroxymonosulfate activation for pollutants degradation: efficiency, mechanism and stability. *Colloids Surf. A* **2022**, *642*, 128674.
34. Gankhuyag, G.; Bae, D. S.; Lee, K.; Lee, S. One-Pot Synthesis of SiO_2@Ag Mesoporous Nanoparticle Coating for Inhibition of Escherichia coli Bacteria on Various Surfaces. *Nanomaterials* **2021**, *11*(2), 549.
35. Chen, Z.; Lu, S.; Zhang, Z.; Huang, X.; Zhao, H.; Wei, J.; Li, F.; Yuan, K.; Su, L.; Xiong, Y. Green photoreduction synthesis of dispersible gold nanoparticles and their direct in situ assembling in multidimensional substrates for SERS detection. *Mikrochim. Acta* **2022**, *189*, 275.
36. Rahman, A.; Kumar, S.; Bafana, A.; Lin, J.; Dahoumane, S.A.; Jeffryes, C. A mechanistic view of the light-induced synthesis of silver nanoparticles using extracellular polymeric substances of *Chlamydomonas reinhardtii*. *Molecules* **2019**, *24*, 3506.